JGR Atmospheres

RESEARCH ARTICLE
10.1029/2022JD038203

On the Polar Bias in Ice Core ^{10}Be Data

F. Adolphi[1,2,3], K. Herbst[4], A. Nilsson[5], and S. Panovska[6]

[1]Alfred Wegener Institute, Helmholtz Centre for Polar and Marine Research, Bremerhaven, Germany, [2]Department of Geosciences, University of Bremen, Bremen, Germany, [3]MARUM—Center for Marine Environmental Sciences, Bremen, Germany, [4]Institut für Experimentelle und Angewandte Physik, Christian-Albrechts-Universität zu Kiel, Kiel, Germany, [5]Department of Geology—Quaternary Sciences, Lund University, Lund, Sweden, [6]GFZ German Research Centre for Geosciences, Section 2.3, Helmholtz Centre Potsdam, Potsdam, Germany

Key Points:

- Mixing-model experiments and independent data suggest that ice-core ^{10}Be-records do not capture a global-mean signal
- During the glacial, modulation by geomagnetic field changes is dampened by ∼23%. Effects of solar activity changes are enhanced by ∼7%
- A transfer function is proposed that restores the approximate proportionality of ice core data to global production rate changes

Supporting Information:

Supporting Information may be found in the online version of this article.

Correspondence to:

F. Adolphi,
florian.adolphi@awi.de

Citation:

Adolphi, F., Herbst, K., Nilsson, A., & Panovska, S. (2023). On the polar bias in ice core ^{10}Be data. *Journal of Geophysical Research: Atmospheres*, *128*, e2022JD038203. https://doi.org/10.1029/2022JD038203

Received 16 NOV 2022
Accepted 8 JAN 2023

Author Contributions:

Conceptualization: F. Adolphi
Data curation: A. Nilsson
Formal analysis: F. Adolphi, K. Herbst, A. Nilsson
Funding acquisition: F. Adolphi
Investigation: S. Panovska
Methodology: F. Adolphi, K. Herbst, A. Nilsson, S. Panovska
Project Administration: F. Adolphi
Visualization: F. Adolphi
Writing – original draft: F. Adolphi
Writing – review & editing: K. Herbst, A. Nilsson, S. Panovska

Abstract Cosmogenic radionuclide records from polar ice cores provide unique insights into past cosmic ray flux variations. They allow reconstructions of past solar activity, space weather, and geomagnetic field changes, and provide insights into past carbon cycle changes. However, all these applications rely on the proportionality of the ice core radionuclide records to the global mean production rate changes. This premise has been long debated from a model and data-perspective. Here, we address this issue through atmospheric mixing model experiments and comparison to independent data. We find that all mixing scenarios, which do not assume complete tropospheric mixing, result in a polar bias. This bias is more prominent for geomagnetic field changes than solar modulation changes. The most likely scenario, supported by independent geomagnetic field records and marine ^{10}Be during the Laschamps geomagnetic field minimum, results in a dampening of geomagnetic field induced changes by 23%–37% and an enhancement of solar-induced changes by 7%–8%. During the Holocene, we do not find conclusive evidence for a polar bias. We propose a correction function that allows deconvolving the glacial ice core record in order to restore proportionality to the global mean signal.

Plain Language Summary Ice core records of cosmogenic radionuclides (e.g., ^{10}Be) are unique archives providing information on past changes in galactic and solar cosmic ray fluxes. The atmospheric production rates vary in response to changes of the cosmic ray flux, which in turn is modulated by solar and geomagnetic shielding. Typically, it is assumed that the deposition of ^{10}Be on the ice varies in proportion to changes in its atmospheric production rate. However, this assumption has been questioned early on, since the geomagnetic shielding against cosmic rays depends on the geomagnetic latitude, being essentially zero at the ice-core locations. It was proposed, that ice cores may suffer from a "polar bias" which dampens the geomagnetic field signal and enhances the solar signal in ice core ^{10}Be, thus questioning the use of ice-core ^{10}Be-data as proxies for global cosmogenic radionuclide production rate changes. Here, we revisit this hypothesis using mixing model experiments in conjunction with a compilation of ^{10}Be data from high and low-latitude archives and geomagnetic field models. We deduce that a polar bias is likely present in glacial ice-core ^{10}Be-records and provide a simple method to approximately restore the proportionality of ice core ^{10}Be data to global production rate changes.

1. Introduction

Ice cores are invaluable archives to constrain past atmospheric production rate changes of cosmogenic radionuclides (CRNs, e.g., ^{10}Be, ^{36}Cl, ^{14}C). The CRN-production rates depend on the incoming flux of cosmic rays which trigger a nuclear cascade in the atmosphere, eventually resulting in CRN production (Lal & Peters, 1967). The cosmic ray flux inside the heliosphere, in turn, depends on the strength of the interplanetary magnetic field, related to solar activity, and the geomagnetic field. Hence, ice-core CRN-records allow the reconstruction of past solar activity and geomagnetic field strength (e.g., Muscheler et al., 2016; Zheng, Sturevik-Storm, et al., 2021). This approach also provides independent estimates of the relative changes of past ^{14}C-production rates which are approximately proportional to those of ^{10}Be (Poluianov et al., 2016), allowing inferences about past carbon cycle changes (Dinauer et al., 2020; Köhler et al., 2022; Muscheler et al., 2004). However, the underlying assumption for all these applications is that the relative changes of CRN-fluxes (or concentrations) measured in ice cores are proportional to the global atmospheric production rate changes. The validity of this assumption is an ongoing topic of debate and different studies based on models and/or data have reached different conclusions on the presence of this so-called "polar bias" (Adolphi et al., 2018; Adolphi & Muscheler, 2016; Bard et al., 1997; Elsässer

et al., 2015; Field et al., 2006; Heikkilä et al., 2009; Mazaud et al., 1994; McCracken, 2004; Pedro et al., 2012; Steig et al., 1996).

The debate arises from the observation that the CRN production in the atmosphere is spatially highly heterogeneous. First, there is an altitudinal gradient of the atmospheric CRN-production: The combined effect of the altitudinal profiles of the primary and secondary proton and neutron fluxes, their energy, and the density of target atoms results in a CRN-production rate maximum in the lower stratosphere and generally decreasing production rates at lower atmospheric levels, such that roughly two-thirds of the global ^{10}Be production occur in the stratosphere and one third in the troposphere (Heikkilä et al., 2009). Second, the Earth's dipole-dominated magnetic field provides no shielding around the geomagnetic poles, where the fieldlines are approximately perpendicular to Earth's surface, as opposed to at the equator, where the shielding is strongest. The combined effect is a CRN-production maximum in the polar stratosphere, and a minimum in the equatorial troposphere.

Besides the global pattern of mean CRN-production rates, their modulation by varying geo- and heliomagnetic field strength is spatially heterogeneous as well: Geomagnetic field changes do not affect the local production rates at the poles where geomagnetic shielding is almost absent but have a significant effect at the equator where the horizontal field-component is strong. On the other hand, solar activity changes predominantly affect CRN production rates at the poles because there, low energy cosmic rays which are most strongly modulated by the heliomagnetic field, are not deflected by the geomagnetic field.

From these observations it becomes clear that, whether or not ice cores (or any other geological archive) can record a signal that is proportional to global production rate changes, depends critically on whether these spatial patterns are being sufficiently homogenized by atmospheric mixing prior to deposition in the archive.

Many of the previous studies that postulated a polar bias were based on single records and very simple mixing models (Bard et al., 1997; Mazaud et al., 1994; Steig et al., 1996), some of which were later on contradicted by collections of higher-resolution records (Pedro et al., 2012). The somewhat more advanced model-experiments by McCracken (2004) were (a) still very simplistic in their consideration of atmospheric transport of aerosols from the stratosphere to the troposphere and within the troposphere and (b) validated using the quantification of the polar bias by Bard et al. (1997) and Steig et al. (1996), which are likely overestimates (Elsässer et al., 2015; Pedro et al., 2012). Complex GCM-experiments however, disagree on the presence of a polar bias (Field et al., 2006; Heikkilä et al., 2009).

Here, we try to critically re-evaluate this assumption on the basis of mixing-model experiments that have been parameterized based on full GCM-experiments (Heikkilä et al., 2009). Our focus is on the validation of the model predictions by comparison to an extensive set of independent CRN-data from ice cores, marine sediments as well as geomagnetic field models. Further, we develop a correction scheme that can be applied to ice core CRN data in order to restore proportionality to global production-rate changes.

2. Materials and Methods

2.1. Production Rate Modeling

The ^{10}Be production rates used in this study have been modeled using the yield functions provided by Poluianov et al. (2016) for each latitude and atmospheric depth. The primary cosmic ray spectrum was based on the Local Interstellar Spectrum by Herbst et al. (2017), modulated using the force-field approximation (Gleeson & Axford, 1968), and assuming a nucleonic ratio of alpha and heavier particles of 30% (Webber & Higbie, 2009). Choosing a more recent value of 35.5% (Koldobskiy et al., 2019) does not affect our results as the impact on the spatial distribution and relative modulation on CRN-production rates is below 1%. The geomagnetic shielding (utilizing the cut-off rigidity) was parameterized according to the polynomial fit provided by Lifton et al. (2014) who modeled cut-off rigidities for different intensities of a geocentric axial dipole field.

2.2. Mixing Model

To simulate the effect of atmospheric mixing we apply a simple box-model. The atmosphere is divided into latitudinal bands of 30° and in troposphere and stratosphere, based on the long-term monthly mean tropopause-height of the NCEP-reanalysis (Kalnay et al., 1996), resulting in six boxes per hemisphere. The choice of the boxes was

Table 1
Mixing Model Parameters

Scenario/Box	0°–30° trop [%]	30°–60° trop [%]	60°–90° trop [%]	0°–30° strat [%]	30°–60° strat [%]	60°–90° strat [%]
Global	100 (13)	100 (17)	100 (7)	100 (5)	100 (32)	100 (26)
H09 60°–90°N	0 (0)	5 (18)	19 (27)	4 (4)	4 (28)	4 (22)
H09 GRIP	1 (3)	3.5 (13)	10 (15)	5 (6)	5 (35)	5 (29)
PB	0 (0)	5 (14)	19 (21)	3 (3)	5 (27)	8 (35)

Note. For each scenario, the numbers state how much of the ^{10}Be produced in a certain box is deposited at the ice core site (%). In brackets, we show how much this fraction in turn contributes to the total deposition at the site, illustrating that even if only a few % of the total ^{10}Be produced in the stratosphere are deposited at the ice-core site, the stratosphere is still the largest contributor to local ^{10}Be-deposition because the stratospheric production rates are very high. For the global scenario, all boxes obtain an equal weight in the mixing model (100%). Thus, the numbers in brackets reflect the relative contribution of each box to the global budget. Note that they are rounded and may hence not add up to 100%. Furthermore, the exact values depend on the exact choice of, for example, the tropospheric height, the solar modulation and the geomagnetic field (see main text and Figure 2). Note that in the following discussion all production rates are normalized. Hence, the absolute numbers for each box are irrelevant but only the ratio between the boxes affects the presented results.

motivated by the study of (Heikkilä et al., 2009) who explicitly modeled the transport and mixing of ^{10}Be in a state-of-the-art Global Circulation Model and reported their results for these boxes (Tables 2 and 3 in Heikkilä et al., 2009) which also roughly correspond to the main atmospheric circulation cells. Their estimate of the fraction of ^{10}Be produced in a given box which is deposited in Greenland serves as a starting point for our mixing model. Hence, our model implicitly accounts for regional differences in aerosol transport and deposition as modeled in the full GCM by Heikkilä et al. (2009). We note that we only considered the stratospheric production in one hemisphere. Hence, we need to double the stratospheric fraction given by Heikkilä et al. (2009) which refers to the whole stratospheric budget. We define four scenarios that are also summarized in Table 1 and Figure 1:

Global: The entire atmosphere is well mixed (all boxes are mixed to equal proportions).

H09 60°–90°N: Based on the results by Heikkilä et al. (2009, henceforth, "H09" in the scenario names) for the ^{10}Be deposition between 60° and 90°N. The stratosphere is well mixed but there is a strong gradient in the troposphere, such that only ^{10}Be produced north of 30°N reaches the northern hemisphere polar areas, while ^{10}Be that is produced in the tropical troposphere does not contribute to the deposition north of 60°N.

H09 GRIP: Also based on the results by Heikkilä et al. (2009) for the ^{10}Be deposition at the GRIP ice core site. The troposphere again shows a strong latitudinal gradient in its contribution to the polar ^{10}Be deposition. However, there is also a small fraction coming from the tropical troposphere. This scenario also assumes a well-mixed stratosphere which also contributes more to the total deposition.

PB: A polar bias scenario in which the tropospheric mixing is similar to H09 60°–90°N but additionally, the stratosphere is not mixed entirely but shows a gradient of increasing contribution to the polar deposition with latitude.

We do not aim to realistically reproduce absolute ^{10}Be deposition-fluxes at a specific ice core site. Instead, this mixing model serves to illustrate the effects of different possible mixing-scenarios on the assumption of proportionality of ice core ^{10}Be records to global production rates. Hence, we only study the relative deposition changes compared to relative production rate changes. This is similar to the most common approaches applied to ice core data, which are typically normalized to reconstruct past production rate changes.

3. Results

3.1. Model Predictions

Figure 1 shows the results from the box model. It can be seen that all scenarios with incomplete mixing lead to a polar bias: All scenarios show a diminished sensitivity of ^{10}Be deposition to geomagnetic field changes compared to the global scenario (Figure 1 bottom right). At the same time, they are characterized by enhanced sensitivities to solar activity changes compared to the global scenario (Figure 1 panel b). We define "sensitivity" as the

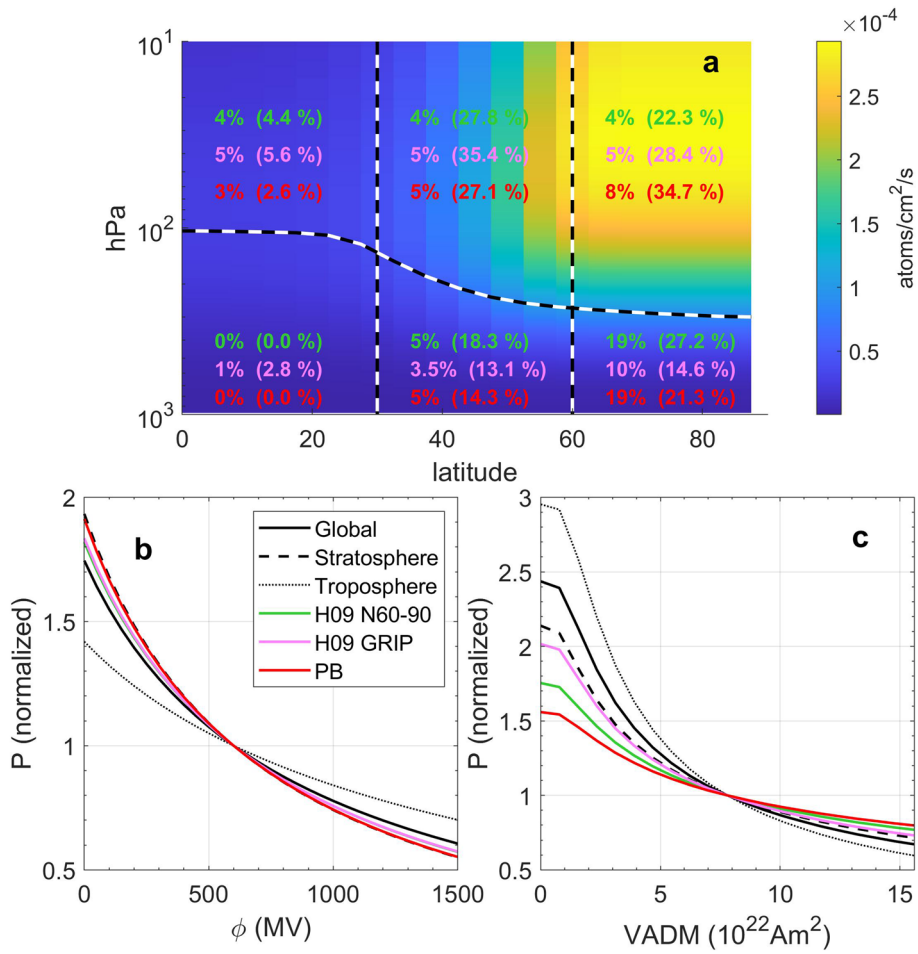

Figure 1. Panel (a) ^{10}Be production rates for a solar modulation potential of 600 MeV and modern geomagnetic field strength. The boxes used in the mixing model are divided by the dashed lines. For each scenario (color-coded as in the legend of panel b and described in Table 1) and box, it is indicated which fraction is exported to the ice core (i.e., how much of the ^{10}Be produced in this box is being deposited at the ice core site) and how much this in turn contributes to the total deposition there (in brackets, i.e., how much of the total ^{10}Be deposited at the ice core site was produced in this box). These numbers differ due to the different inventories of each box. For the global scenario the numbers are only given in Table 1 but omitted here for clarity. Panel (b) Simulated deposition change for each mixing scenario as a function of solar activity. Panel (c) Simulated deposition change for each mixing scenario as a function of geomagnetic field strength.

relative CRN-production rate change in response to a given change in solar modulation/geomagnetic field intensity. However, the attenuation/enhancement effect is not similar for geomagnetic and heliomagnetic modulation of the GCR-flux. The sensitivity to solar changes is only enhanced by up to 15% while the sensitivity to geomagnetic field changes is reduced by up to 47% of the global value. These estimates agree with an earlier study using a more complex transport model (Elsässer et al., 2015) and rule out extreme polar bias scenarios as proposed by Bard et al. (1997), who inferred a solar enhancement of 53%. This would result in an even stronger suppression of the geomagnetic field signal in ice core CRN-records and can be ruled out by comparing ^{10}Be-records to independent estimates of geomagnetic field strength during the Laschamps geomagnetic field minimum (Adolphi et al., 2018; Muscheler et al., 2005).

To understand this difference in the response to geomagnetic and solar changes, it is instructive to look at the changes in the spatial distribution of atmospheric CRN-production rates (Figure 2). Solar modulation affects mainly the stratospheric CRN-production-rates. During solar minima, the stratospheric production rate changes at each latitude range from 20% to 170% of the global mean change (Figure 2k). However, the long residence time of ^{10}Be in the stratosphere of 1–2 years allows for sufficient mixing and homogenization of these differences (Heikkilä et al., 2009; Raisbeck et al., 1981). Empirical evidence for this efficient stratospheric mixing

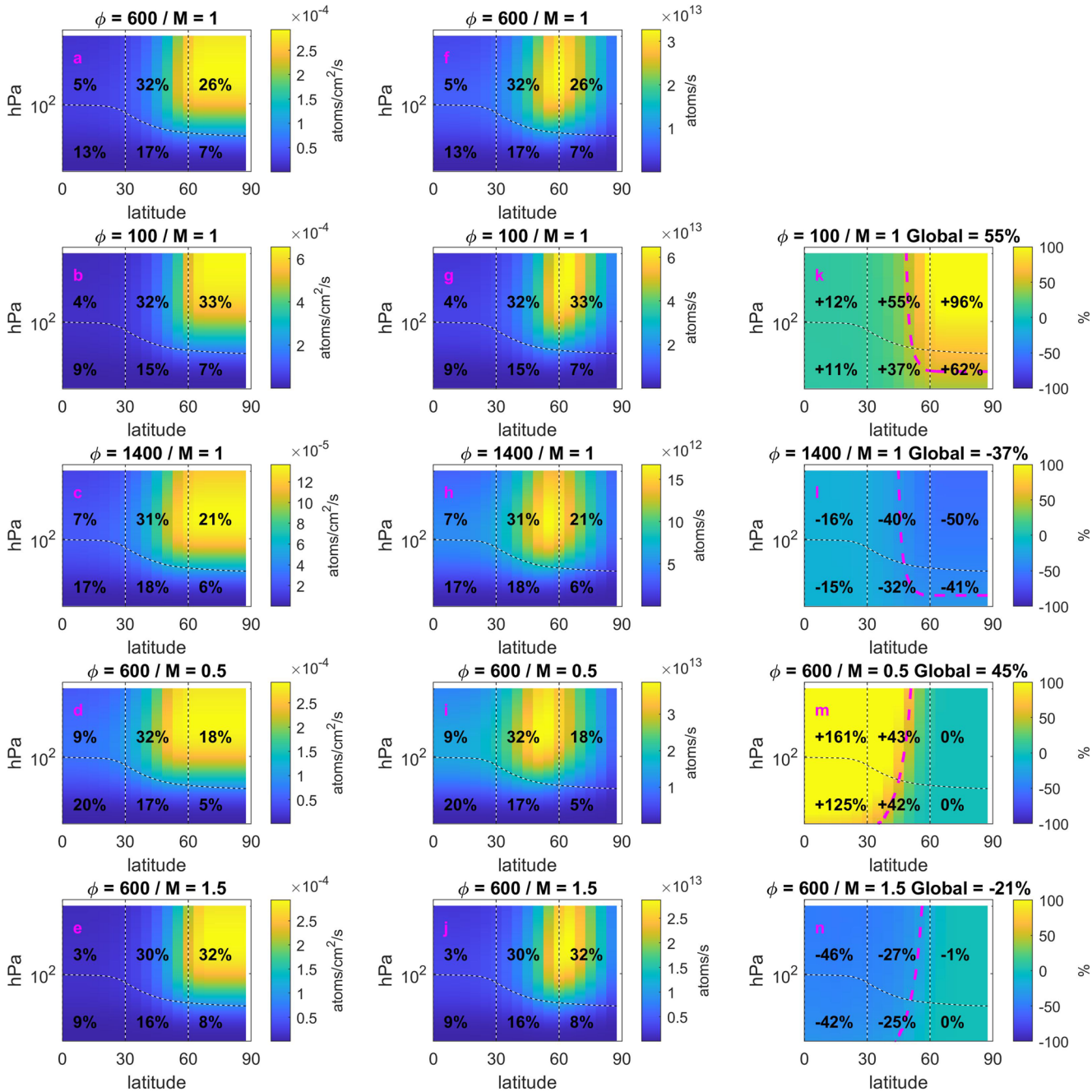

Figure 2. Spatially resolved (atmospheric height, latitude) ^{10}Be production rate changes for different levels of solar activity (Φ) and geomagnetic field strength relative to today (M). On top of each panel, the applied solar modulation potential (Φ [MV]) and geomagnetic field strength (relative to today) are indicated. Left (a–e): Production rates in atoms/cm^2/s. Middle (f–j): Production rates in atoms/s (i.e., multiplied by the surface-area of each grid-cell). Right (k–n): relative production rate change [% deviation from the production rates at Φ = 600 MV and $M = 1$, see top row panels] for each point in space (5° latitude). The magenta dashed line is the isoline of the globally averaged change which is also indicated on top of each panel. The numbers in each box indicate their contribution to the global budget (left and middle panel) or the averaged production rate change in this box (right).

comes from the short-term production rate increases in ^{10}Be and ^{14}C during Solar Energetic Particle-events (SEPs; Büntgen et al., 2018; Mekhaldi et al., 2015; Miyake et al., 2012). Their excess-production is confined to the polar stratosphere, and yet, ice-core ^{10}Be records do not record an enhanced signal compared to ^{14}C. On the contrary, the SEP-related changes in ^{10}Be are about 20% smaller than in ^{14}C, possibly due to uncertainties in the production yield functions (Paleari et al., 2022). In the troposphere on the other hand, the latitudinal gradient of CRN-production-rate changes resulting from solar modulation changes is smaller and restricted to

about 20%–110% of the global mean value and the production rate changes in the polar troposphere are comparable to the global mean signal. Hence, assuming that ice cores receive ^{10}Be from a well-mixed stratosphere and the mid-to high-latitude troposphere, a considerable enhancement of solar production rate changes cannot be expected.

In comparison, geomagnetic field changes induce large production rate changes in the tropical and sub-tropical atmosphere (Figures 2m and 2n), and the latitudinal differences in modulation strength are larger than for solar activity changes. For a halving of today's geomagnetic field intensity, they reach from 0% to 360% of the global mean value (Figure 2m). While the stratospheric gradient can be homogenized, the tropospheric residence time of ^{10}Be is too short (1–2 months) to allow for full mixing and only a minor fraction may reach the polar troposphere via upwelling to the stratosphere (Heikkilä et al., 2009). However, in this scenario the contribution of the tropical troposphere to global production increases from 13% to 20%. The tropical tropospheric production rate changes thus become an important term in the global budget that is strongly modulated. Thus, by not sampling this reservoir, ice core CRN-records record a significantly smaller production rate change than the global mean in all mixing scenarios. We note that even if ice cores only received ^{10}Be from a well-mixed stratosphere, they would underestimate the global production rate change because the modulation in the stratosphere is smaller than the global mean (Figure 1). The addition of a potential regional (polar) tropospheric contribution which is not modulated at all reduces the recorded ^{10}Be-change even further.

3.2. Devising a Spectral Correction Scheme

As shown above, a polar bias has different consequences on ^{10}Be deposition, depending on whether production rate changes are driven by changes in solar modulation or the geomagnetic field. Here, we propose a correction scheme based on the finding that solar activity and the geomagnetic field dominate production rate changes on different timescales (Snowball & Muscheler, 2007). Previously, this characteristic has been used to isolate one or the other process by applying hard frequency cut-offs (Adolphi et al., 2014; Muscheler et al., 2005; Zheng, Sturevik-Storm, et al., 2021). Here, we develop a filter approach that can simultaneously correct average biases arising from both processes, which can be advantageous especially when one is not necessarily interested in the specific modulation process but the global CRN-production rate changes.

First, we describe solar modulation and geomagnetic field intensity changes in the form of a frequency spectrum. For changes in solar modulation, we use a smoothed average (Savitzki-Golay filter) of the individual spectra of different solar activity reconstructions (see Figure 3, left). For geomagnetic field intensity variations, we approximate the average spectrum by fitting a piecewise linear function with spectral slopes $f^{-\alpha}$ of $\alpha = 0$, 2, and 4 and corner frequencies of 3×10^{-5} and 3×10^{-3} a^{-1} (Figure 3, right; Bouligand et al., 2016; Buffett & Matsui, 2015). As we will see later, the exact shape of the spectra is only important in the frequency range, where solar modulation and geomagnetic field strength both contribute significantly to the CRN-production rate changes, that is, 2×10^{-4} to 2×10^{-3} a^{-1} (wavelengths of 500–5,000 years). On longer (shorter) wavelengths the CRN production rates are clearly dominated by geomagnetic field intensity (solar activity) and then, the exact shape of the spectrum becomes unimportant for the correction factor.

Subsequently, we generate 1,000 random realizations of these spectra with random phases uniformly sampled from $-\pi$ to π and a squared amplitude sampled from a χ^2-distribution with 2 degrees of freedom around the prescribed spectrum (Wilks, 2006). These random samples of the prescribed spectra are then transformed into timeseries by inverse Fast Fourier Transform. From each noise series, we subtract its minimum so that the resulting 1,000 random solar modulation records and 1,000 random geomagnetic field intensity records cannot reach unphysical negative values (see Figure 3, lower panels for examples). The resulting mean $\pm$1 sigma of all noise series is 450 $\pm$ 15 MeV and 8.5 $\pm$ 1 $\times 10^{22}$ Am^2 for solar modulation and geomagnetic field intensity, respectively, which fall within the range of the available reconstructions.

Using these random solar modulation and geomagnetic field records, we modeled ^{10}Be production rates and the expected ice-core signal according to the different mixing scenarios described in Section 2.2 and Table 1.

Figure 4 shows how the different mixing scenarios affect the proportionality of the synthetic ice-core record compared to the global mean signal of CRN-production rate changes. We can define an amplitude enhancement factor as a function of frequency for each mixing scenario by dividing the corresponding power spectrum by the spectrum of the global mean production rates. On long timescales (>5,000 years or a frequency of 2×10^{-4} a^{-1}) the production rate changes are exclusively driven by geomagnetic field changes. There, the mixing model yields

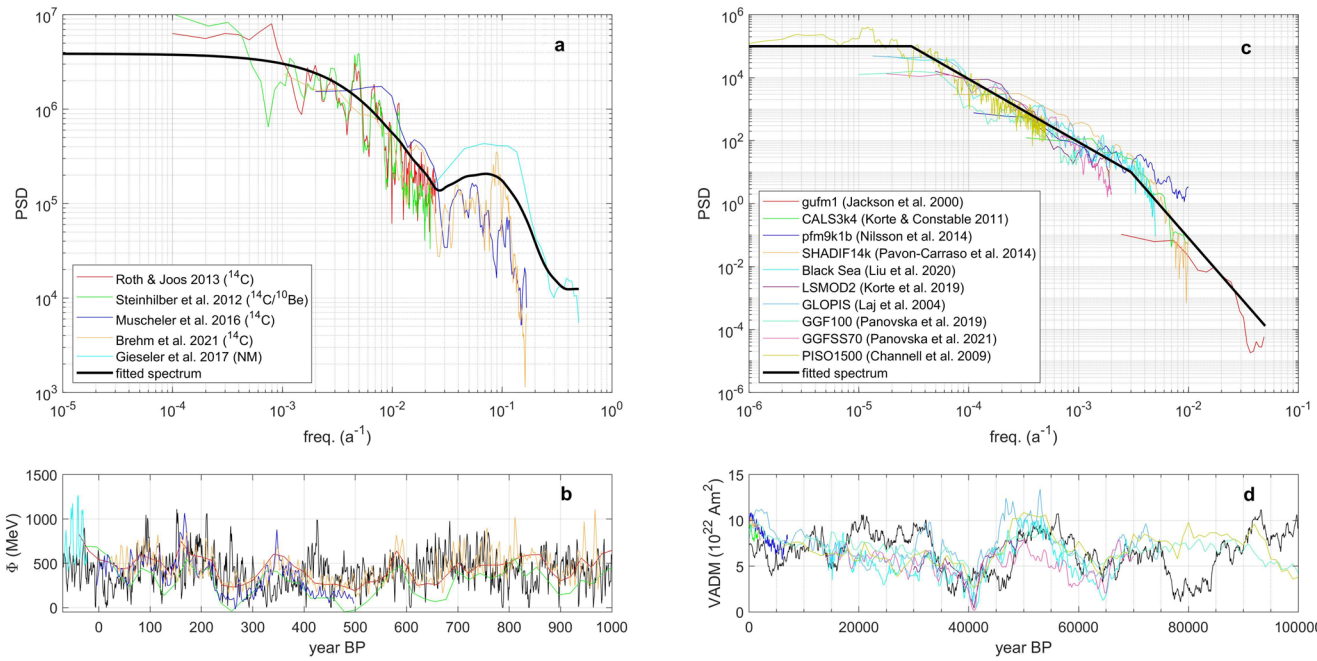

Figure 3. Spectra of solar modulation changes (a) (Brehm et al., 2021; Gieseler et al., 2017; Muscheler et al., 2016; Roth & Joos, 2013; Steinhilber et al., 2012) and geomagnetic field intensity changes (c) (Channel et al., 2009; Jackson et al., 2000; Korte & Constable, 2011; Korte et al., 2019; Laj et al., 2004; Liu et al., 2020; Nilsson et al., 2014; Panovska et al., 2019, 2021; Pavon-Carraso et al., 2014). Each colored line represents a different reconstruction from the literature. The bold black line shows the fitted spectrum used to generate random realizations of both quantities. The lower panels show the reconstructions of solar activity (b) and geomagnetic field intensity (d) as timeseries (colored as above) including one random realization (black) of the fitted spectrum. PSD denotes "power spectral density".

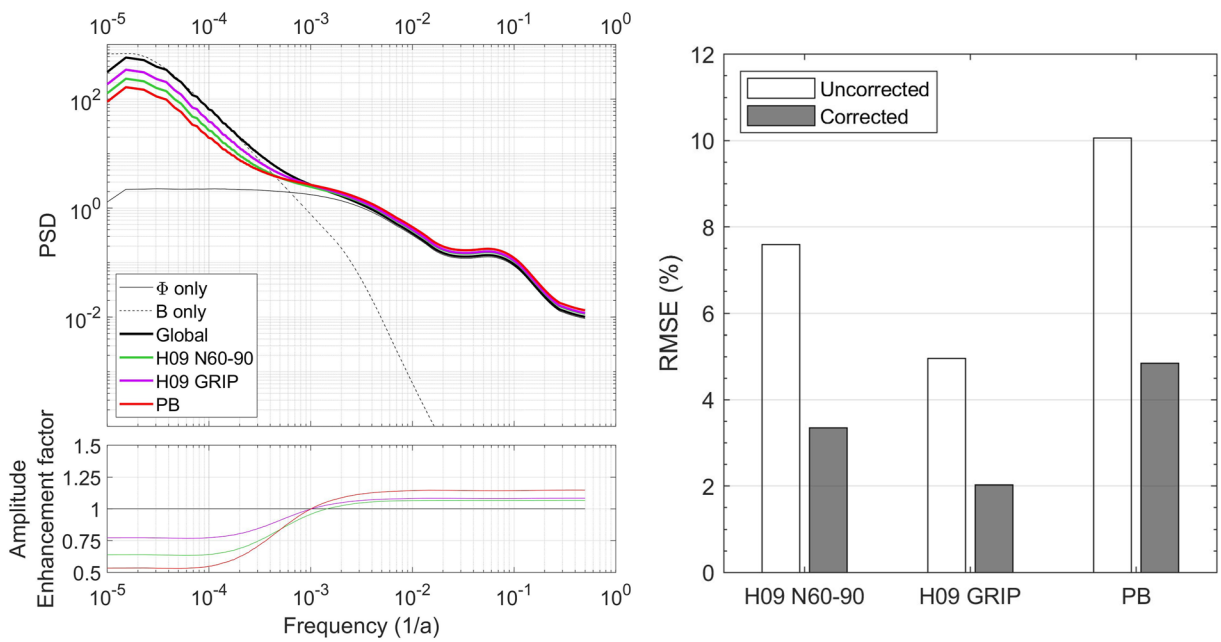

Figure 4. Left: Mean frequency spectra of the 1,000 simulated CRN-deposition records according to the different mixing model scenarios (top left), and inferred amplitude enhancement factor (bottom left) when comparing the mixing model output to the global mean signal. Right: Mismatch of the mixing model output and the global mean CRN production rate quantified as a root mean square error (RMSE, white bars). The gray bars show the RMSE of the mixing model output and the global mean production rate after applying the spectral correction scheme described in the text.

an amplitude-reduction of 23%–47% of the recorded CRN-production rate changes compared to the global mean signal (Figure 4 lower panel). On shorter periods (<500 years or a frequency of 2×10^{-3} a^{-1}), solar modulation is the sole driver of production rate changes. Here, the amplitude enhancement is moderate, between 7% and 15%. Between 500 and 5,000 years, both processes contribute to the modulation of CRN-production rates. Hence, this ambiguity leads to a smooth transition between enhancement and dampening.

The defined amplitude enhancement factor can be used to restore proportionality from the mixed signal (i.e., ice core) by calculating the power spectrum of the ice-core record, dividing its amplitudes by the enhancement factor, and converting it back into a timeseries by inverse Fourier transform. Figure 4 (right) illustrates the effect of applying this correction to the synthetic ice core record: Initially, the root mean square error (RMSE) between the simulated ice core and global mean production rate changes amounts to 5%–10%. After applying the correction, the RMSE is approximately halved for each mixing scenario. The remaining mismatch arises from the previously described ambiguity of the origin of production rate changes on timescales between 500 and 5,000 years. Without prior knowledge of the origin of production rate changes this cannot be rectified accurately for each oscillation, since the correction is purely statistical and not mechanistic.

3.3. Comparison to Independent Data

So far, the considerations presented here are merely theoretical but strongly suggest, that a polar bias can be expected to be present in ice core ^{10}Be records from polar regions. In this section, we compare the ^{10}Be ice core stack compiled by Adolphi et al. (2018) and corrected in Köhler et al. (2022) to a suite of independent data sets. We focus on the Laschamps geomagnetic field minimum around 41 kaBP (Bonhomme & Babkine, 1967) which provides good data coverage from ice core and marine ^{10}Be records and geomagnetic field reconstructions. As shown in the previous section, the effect of a polar bias can be expected to be most prominent for production rate changes induced by changes in the geomagnetic field, while it is less pronounced for solar modulation. Hence, we can expect the best "signal to noise" for this most recent period, when the geomagnetic dipole moment approach values close to zero (Korte et al., 2019). One caveat is the increasing importance of non-dipole moments when the dipole field approaches zero. However, we indirectly address this issue by also comparing to marine ^{10}Be records, which will be affected by geomagnetic shielding in a similar way while being less sensitive to incomplete atmospheric mixing due to additional mixing in the ocean. Furthermore, Greenland and Antarctic ice core ^{10}Be-records show increases of similar amplitude during the Laschamps. This implies that the production-rate patterns arising from non-dipole moments must be homogenized by atmospheric mixing prior to deposition because we don't expect the same non-dipole shielding in both hemispheres. Conducting the same comparison between modern neutron monitor and ice-core ^{10}Be data yields inconclusive results, because the expected enhancement is of similar magnitude as the ^{10}Be measurement error and the difference between individual sites (Figure S1).

First, we compare the ice core record to a suite of marine ^{10}Be-records (Figure 5). Marine ^{10}Be records have (for this purpose) the advantage that Beryllium has an oceanic residence time of roughly 200–1,000 years, depending on location (Ku et al., 1990; Kusakabe et al., 1990; von Blanckenburg et al., 1996). This additional mixing time allows for a more complete homogenization of ^{10}Be-production patterns prior to deposition, compared to atmospheric records such as ice cores. Nearly all investigated marine ^{10}Be records show a larger production rate increase than the uncorrected ice-core stack, supporting the presence of a polar bias. Only the record from ODP 983 in the northern North Atlantic (Christl et al., 2010) shows a lower production rate increase. This record, however, required a correction for the lateral transport of ^{10}Be, which reduces the amplitude of ^{10}Be deposition changes compared to the normalization using Th-excess measurements only (Christl et al., 2010). The average ^{10}Be-deposition change of all other investigated marine records is most compatible with our mixing model scenarios of a weak polar bias (H09 GRIP and H09 N60°–90°).

In addition, we compare the ice core CRN-Stack to independent reconstructions of geomagnetic field intensity variations (Figure 6). For this purpose, we calculated the expected atmospheric ^{10}Be production rate changes from the geomagnetic field records and global models assuming a constant solar modulation of 500 MeV. Subsequently, we applied the mixing model to create virtual ice core records expected for each mixing scenario, which can then be compared to the measured ice core data.

Congruent to the comparison to marine ^{10}Be (Figure 5), the geomagnetic field records yield larger production rate changes than the ice core stack and only become compatible with the ice core data when incomplete tropospheric mixing is assumed.

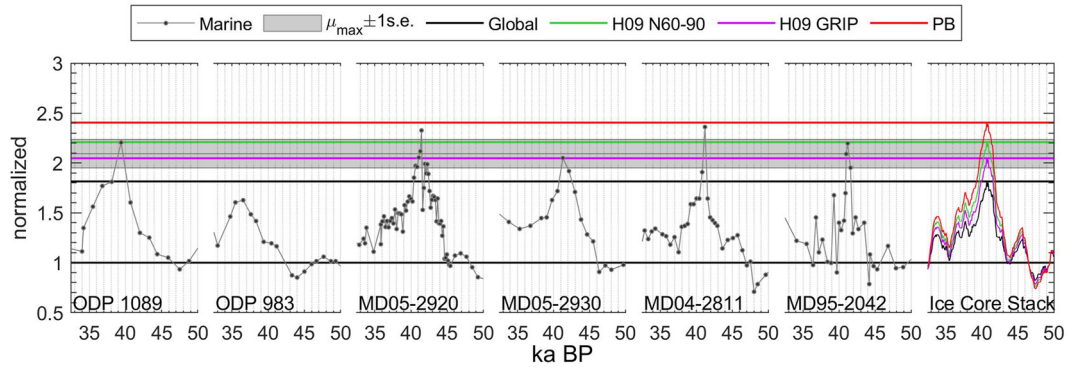

Figure 5. Comparison of marine ^{10}Be records from the South Atlantic (ODP 1089, Christl et al., 2007), North Atlantic (ODP 983, Christl et al., 2010), western equatorial Pacific (MD05-2920, Simon et al., 2020), the Gulf of Papua (MD05-2930, Simon et al., 2016), and Iberian Margin (MD95-2042, Carcaillet et al., 2004; MD04-2811, Ménabréaz et al., 2011) to the ice core radionuclide stack (Adolphi et al., 2018). The gray band encompasses the mean of the ^{10}Be maxima seen in the marine records plus-minus its standard error. The ice core data has been smoothed in order to account for a ∼400 year residence time of Beryllium in the ocean following Christl (2007). All records have been normalized to their mean prior to the Laschamps event from 45 to 50 ka BP in order to quantify the relative production rate increase associated with the geomagnetic field minimum.

While differences between all datasets make it challenging to decide whether scenario H09 N60–90 or H09 GRIP provides a better fit to the independent ^{10}Be data from marine sediments and geomagnetic field reconstructions, we can still rule out the scenarios that assume either full global mixing or incomplete mixing in the stratosphere.

For the Holocene period, we compare the ice core data to production rate estimates based on a range of geomagnetic field models (Constable et al., 2016; Nilsson et al., 2014; Pavón-Carrasco et al., 2014), and modeled ^{14}C production rates (Roth & Joos, 2013). Atmospheric ^{14}C is well-mixed and thus, provides an independent estimate of global CRN-production, modulated by the same processes as ^{10}Be, but not affected by the same mixing and transport effects. However, it requires a carbon cycle model to deconvolve the influences of carbon-cycle and production-rate changes on atmospheric ^{14}C/^{12}C (Siegenthaler et al., 1980). Hence, ^{14}C-production rate estimates rely on accurate knowledge and simulation of the past carbon cycle, which are challenging especially during the glacial (e.g., Dinauer et al., 2020). During the climatically more stable Holocene, these effects can be expected to be less variable, albeit not negligible (Roth & Joos, 2013; Vonmoos et al., 2006).

The comparison between these datasets is shown in Figure 7. The ice core CRN-data agrees well with ^{14}C but implies larger variations than most geomagnetic field models. Assuming incomplete atmospheric mixing of ^{10}Be

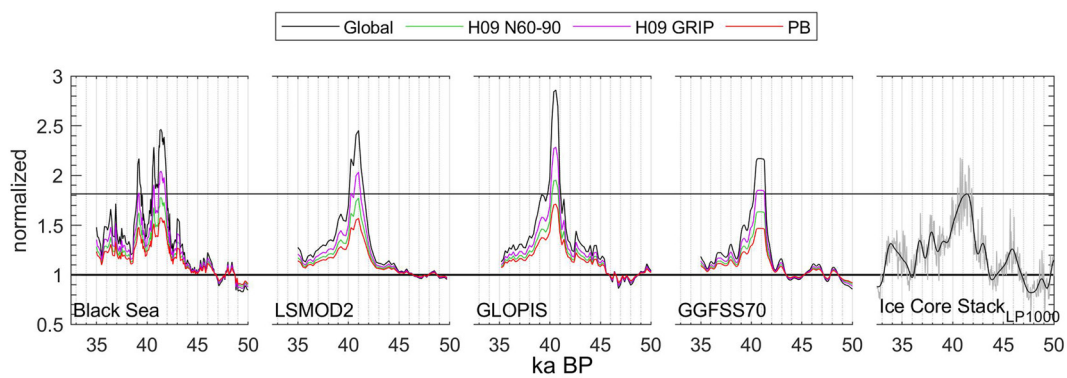

Figure 6. Comparison of modeled ^{10}Be deposition rate changes based on geomagnetic field intensity reconstructions and the mixing model to the ice core CRN stack (Adolphi et al., 2018). Results are shown for geomagnetic field reconstructions from Black Sea sediments (Liu et al., 2020), and different global compilations and models (Korte et al., 2019; Laj et al., 2004; Panovska et al., 2021). All records have been normalized to their mean prior to the Laschamps event from 45 to 50 ka BP in order to quantify the relative production rate increase associated with the geomagnetic field minimum. The ice core data have been smoothed using a 1,000 year low-pass filter in order to highlight production rate changes induced by the geomagnetic field. The horizontal black lines highlight the amplitude of the production rate change seen in ice cores.

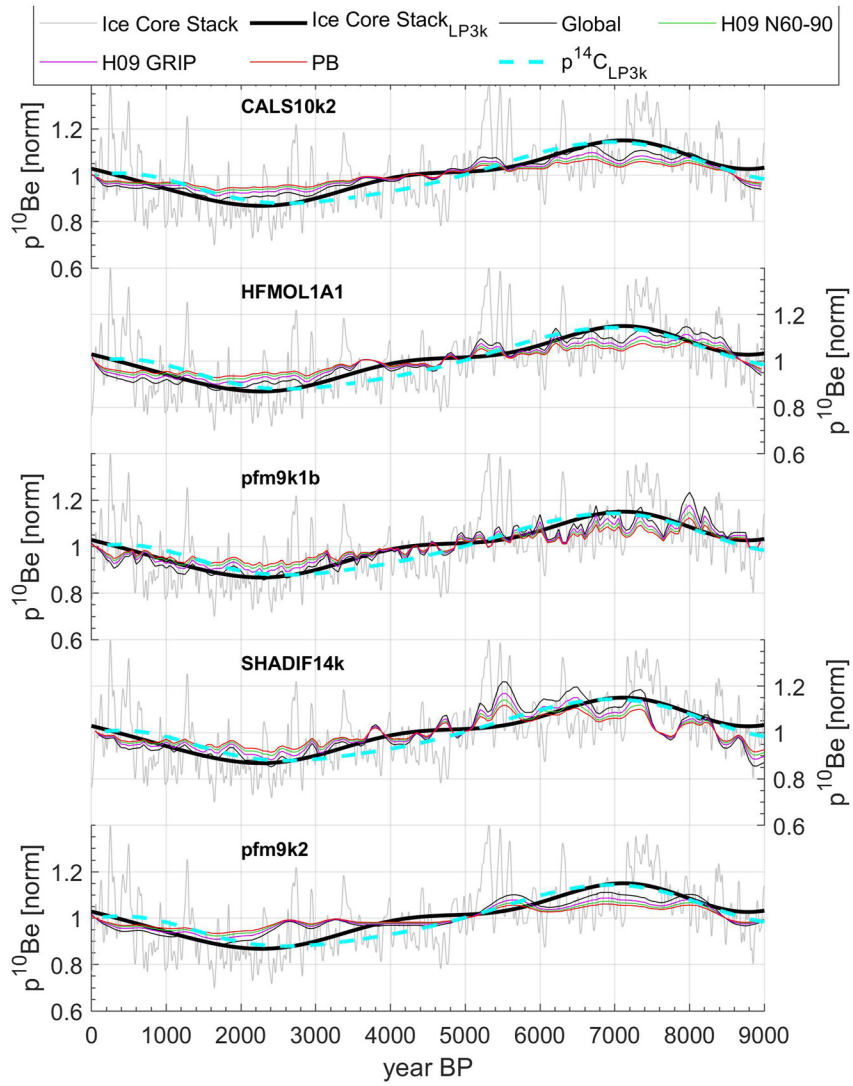

Figure 7. Comparison between the ice core CRN stack (gray and bold black), modeled ^{14}C-production rates (dashed cyan, Roth & Joos, 2013), and modeled ^{10}Be production rates from different geomagnetic field models for the Holocene (CALS10k2 and HFMOL1A1: Constable et al., 2016; pfm9k1b: Nilsson et al., 2014; SHADIF14k: Pavón-Carrasco et al., 2014; pfm9k2: Nilsson et al., 2022) and according to the different mixing scenarios (colored lines, legend). The ice core data is shown unfiltered (light gray) and filtered with a 3,000 year low-pass (bold dark gray). All records have been normalized to their mean between 500 and 9,000 years BP.

(i.e., a polar bias) leads to increased differences to geomagnetic field models and ^{14}C-production rates. To explain these observations, we can formulate four main hypotheses.

i) The Holocene geomagnetic field models underestimate the amplitude of the actual intensity changes.
ii) The difference between ^{10}Be (and ^{14}C) and geomagnetic field models results from solar modulation of CRN-production rates.
iii) The atmospheric mixing of ^{10}Be differs between the glacial and the Holocene, which results in a polar bias during the ice-age but not during the recent warm-period.
iv) Non-dipole shielding during the Laschamps is significant, and hence, production rate changes modeled from geomagnetic field records are overestimated by dipole-only models leading to an overestimate of the polar bias in ice core data.

Hypothesis i) is supported by the agreement of ^{10}Be and ^{14}C and may arise from a loss of variance when combining a large number of records. Furthermore, the models by (Nilsson et al., 2014) and (Pavón-Carrasco et al., 2014) almost reach the amplitude implied by the CRN.

Hypothesis ii) requires solar activity changes that are in-phase with geomagnetic field changes, which seems unlikely.

Hypothesis iii) is supported by the increased mismatch of ice-core CRN-records to ^{14}C and geomagnetic field changes when incomplete mixing of ^{10}Be is assumed (i.e., all scenarios except "global"). The global mixing scenario provides the best fit between all records during the Holocene. Yet, this is in disagreement with the modeling by Heikkilä et al. (2013), who showed that the mixing of ^{10}Be is relatively similar during the glacial and the Holocene. On the contrary, the drier atmosphere and longer atmospheric residence time of aerosols would lead to more latitudinal mixing during the glacial compared to the Holocene. Similarly, a lower tropopause height during colder climates would lead to an increased fraction of stratospheric ^{10}Be and, hence, better latitudinal mixing during the glacial. Tropospheric circulation changes during the glacial, on the other hand, were different in both hemispheres, and yet, the ^{10}Be-changes in Arctic and Antarctic ice cores around Laschamps agree in amplitude. In our model-scenario with the smallest polar bias (H09 GRIP), we need to increase the contribution of ^{10}Be produced in the tropical troposphere by a factor of 4–5 for the polar bias to vanish. This would likely require increased upwelling of tropical tropospheric airmasses into the stratosphere (Heikkilä et al., 2009), possibly facilitated by a more vigorous Brewer-Dobson circulation during modern times compared to the glacial (Fu et al., 2020).

Hypothesis iv) implies that our inference of a polar bias during the glacial is an artifact resulting from overestimated production-rate changes from geomagnetic field models, which in reality have been smaller due to a residual shielding provided by higher moments of the geomagnetic field. Recent studies have shown that during the Laschamps non-dipole moments of the field become important (Korte et al., 2019; Panovska et al., 2021). These moments translate into effective cutoff-rigidities of ∼1.5 GV with a relatively uniform latitudinal and longitudinal structure (Gao et al., 2022). This is supported by the similar amplitude of ^{10}Be-deposition changes in Greenland and Antarctica, which would differ if there were significant latitudinal dependencies of the residual shielding by the non-dipole field. Assuming a globally uniform effective cutoff-rigidity of 1.5 GV leads to an 8% reduction of the modeled global ^{10}Be production rates compared to no geomagnetic shielding (i.e., a dipole-only field during Laschamps). This value is relatively small because the deflected low-energy cosmic rays have low production yields (Poluianov et al., 2016). Importantly, this value is significantly smaller than the difference between the ice-core ^{10}Be data and the prediction by geomagnetic field models which is in the order of 20%–30%, depending on the geomagnetic field model (Figure 6). Lastly, a significant reduction of the expected ^{10}Be production rate changes during Laschamps would lead to an improved agreement between ice cores and geomagnetic field models, but would increase the disagreement to the marine ^{10}Be records.

Taking the evidence from Holocene geomagnetic field models and ^{14}C together, likely points to a combination of hypotheses i) and iii) above. Hypothesis iv) clearly requires further investigation but is unlikely to reconcile all records. The larger amplitude of changes in ^{14}C and ice-core CRN-data, compared to the geomagnetic field models points to some smoothing of the latter. In addition, all mixing-model scenarios that assume incomplete mixing of ^{10}Be lead to an increased mismatch to ^{14}C and the geomagnetic field models. This points to more complete tropospheric mixing of ^{10}Be during the Holocene compared to the glacial and requires further studies employing more detailed atmospheric models.

4. Conclusion

We presented considerations regarding the consequences of incomplete mixing of ^{10}Be in the atmosphere prior to deposition in ice cores and addressed the long-standing debate of a polar bias. By conducting simple mixing model experiments, we find that a polar bias is to be expected as long as the troposphere is not fully mixed. In agreement with Elsässer et al. (2015), we infer that the polar dampening of production rate changes caused by geomagnetic field variations is larger than the enhancement of changes related to solar modulation. This arises from the significant production rate changes in the tropical troposphere during geomagnetic field changes that become a major term in the global budget during geomagnetic field minima, which are not contributing to the polar deposition of ^{10}Be. On the other hand, solar activity changes cause production rate changes that are less spatially heterogeneous and mainly affect the well-mixed stratosphere.

Comparison to independent ^{10}Be data from marine sediments and geomagnetic field reconstructions supports these findings for the last glacial. The best match between these data and ice cores is obtained when a complete

mixing of the stratosphere, but incomplete mixing of the troposphere is assumed. This results in a polar dampening of geomagnetic field-induced production rate changes by 23%–37% and an enhancement of solar modulation-related changes by only 7%–8% (for scenarios H09 GRIP and H09 N60-90, respectively).

During the Holocene, we find a mismatch between geomagnetic field changes and ice core ^{10}Be-records that cannot be reconciled by assumptions about atmospheric mixing and rather point to the absence of a polar bias during the Holocene, and a smoothing in geomagnetic field reconstructions.

We propose a simple correction function that can be applied to the ice core records to restore the proportionality of ice core CRN-records to global production rate changes. Since this method is purely statistical, it cannot correct specific production rate oscillations but will remove average biases. One effect of such a correction is, that it increases the amplitude of multimillennial production rate changes obtained from ice cores, bringing also ice core ^{10}Be and independent ^{14}C records close together during the glacial, albeit not enough to reconcile current disagreements (Dinauer et al., 2020; Köhler et al., 2022).

Data Availability Statement

All data used in this study are available in the cited publications. Ice-core ^{10}Be-data: Adolphi et al. (2018). Marine ^{10}Be-data: Christl et al. (2007), Christl et al. (2010), and Simon et al. (2020). Geomagnetic field reconstructions: Liu et al. (2020), Korte et al. (2019), Laj et al. (2004), Panovska et al. (2021), Constable et al. (2016), Nilsson et al. (2014), Pavón-Carrasco et al. (2014), and Nilsson et al. (2022). The yield functions for calculating ^{10}Be-production rates: Poluianov et al. (2016). The spectral correction function shown in Figure 4 and a Matlab-script how to apply it are available at https://doi.org/10.5281/zenodo.6947463.

Acknowledgments
FA was supported by the Helmholtz Association (VH-NG-1501). AN was supported by the Swedish Research Council (2020–04813). KH acknowledges the support of the DFG priority program SPP 1992 "Exploring the Diversity of Extrasolar Planets (HE 8392/1-1)". S. Panovska acknowledges the Discovery Fellowship at the GFZ Potsdam. Open Access funding enabled and organized by Projekt DEAL.

References

Adolphi, F., Bronk Ramsey, C., Erhardt, T., Lawrence Edwards, R., Cheng, H., Turney, C. S. M., et al. (2018). Connecting the Greenland ice-core and U/Th timescales via cosmogenic radionuclides: Testing the synchroneity of Dansgaard-Oeschger events [Dataset]. Climate of the Past, *14*(11), 1755–1781. https://doi.org/10.5194/cp-14-1755-2018

Adolphi, F., & Muscheler, R. (2016). Synchronizing the Greenland ice core and radiocarbon timescales over the Holocene-Bayesian wiggle-matching of cosmogenic radionuclide records. *Climate of the Past*, *12*(1), 15–30. https://doi.org/10.5194/cp-12-15-2016

Adolphi, F., Muscheler, R., Svensson, A., Aldahan, A., Possnert, G., Beer, J., et al. (2014). Persistent link between solar activity and Greenland climate during the Last Glacial Maximum. *Nature Geoscience*, *7*(9), 662–666. https://doi.org/10.1038/ngeo2225

Bard, E., Raisbeck, G. M., Yiou, F., & Jouzel, J. (1997). Solar modulation of cosmogenic nuclide production over the last millennium: Comparison between 14C and ^{10}Be records. *Earth and Planetary Science Letters*, *150*(3–4), 453–462. https://doi.org/10.1016/s0012-821x(97)00082-4

Bonhomme, N., & Babkine, J. (1967). SUR LA PRESENCE DAIMANTATIONS INVERSEES DANS LA CHAINE DES PUYS. *Comptes Rendus Hebdomadaires des Seances de l'Academie des Sciences, Serie A B*, *264*(1), 92.

Bouligand, C., Gillet, N., Jault, D., Schaeffer, N., Fournier, A., & Aubert, J. (2016). Frequency spectrum of the geomagnetic field harmonic coefficients from dynamo simulations. *Geophysical Journal International*, *207*(2), 1142–1157. https://doi.org/10.1093/gji/ggw326

Brehm, N., Bayliss, A., Christl, M., Synal, H.-A., Adolphi, F., Beer, J., et al. (2021). Eleven-year solar cycles over the last millennium revealed by radiocarbon in tree rings. *Nature Geoscience*, *14*, 10–15. https://doi.org/10.1038/s41561-020-00674-0

Buffett, B., & Matsui, H. (2015). A power spectrum for the geomagnetic dipole moment. *Earth and Planetary Science Letters*, *411*, 20–26. https://doi.org/10.1016/j.epsl.2014.11.045

Büntgen, U., Wacker, L., Galván, J. D., Arnold, S., Arseneault, D., Baillie, M., et al. (2018). Tree rings reveal globally coherent signature of cosmogenic radiocarbon events in 774 and 993 CE. *Nature Communications*, *9*(1), 3605. https://doi.org/10.1038/s41467-018-06036-0

Carcaillet, J., Bourlès, D. L., Thouveny, N., & Arnold, M. (2004). A high resolution authigenic ^{10}Be/9Be record of geomagnetic moment variations over the last 300 ka from sedimentary cores of the Portuguese margin. *Earth and Planetary Science Letters*, *219*(3), 397–412. https://doi.org/10.1016/S0012-821X(03)00702-7

Channell, J. E. T., Xuan, C., & Hodell, D. A. (2009). Stacking paleointensity and oxygen isotope data for the last 1.5 Myr (PISO-1500). *Earth and Planetary Science Letters*, *283*(1), 14–23. https://doi.org/10.1016/j.epsl.2009.03.012

Christl, M. (2007). Sensitivity and response of beryllium-10 in marine sediments to rapid production changes (geomagnetic events): A box model study. *Geochemistry, Geophysics, Geosystems*, *8*(9), Q09015. https://doi.org/10.1029/2007GC001598

Christl, M., Lippold, J., Steinhilber, F., Bernsdorff, F., & Mangini, A. (2010). Reconstruction of global ^{10}Be production over the past 250ka from highly accumulating Atlantic drift sediments [Dataset]. Quaternary Science Reviews, *29*(19–20), 2663–2672. https://doi.org/10.1016/j.quascirev.2010.06.017

Christl, M., Mangini, A., & Kubik, P. W. (2007). Highly resolved beryllium-10 record from ODP site 1089—A global signal? [Dataset]. Earth and Planetary Science Letters, *257*(1–2), 245–258. https://doi.org/10.1016/j.epsl.2007.02.035

Constable, C., Korte, M., & Panovska, S. (2016). Persistent high paleosecular variation activity in southern hemisphere for at least 10 000 years [Dataset]. Earth and Planetary Science Letters, *453*, 78–86. https://doi.org/10.1016/j.epsl.2016.08.015

Dinauer, A., Adolphi, F., & Joos, F. (2020). Mysteriously high I14C of the glacial atmosphere: Influence of 14C production and carbon cycle changes. *Climate of the Past*, *16*(4), 1159–1185. https://doi.org/10.5194/cp-16-1159-2020

Elsässer, C., Wagenbach, D., Levin, I., Stanzick, A., Christl, M., Wallner, A., et al. (2015). Simulating ice core ^{10}Be on the glacial-interglacial timescale. *Climate of the Past*, *11*(2), 115–133. https://doi.org/10.5194/cp-11-115-2015

Field, C. V., Schmidt, G. A., Koch, D., & Salyk, C. (2006). Modeling production and climate-related impacts on^{10}Be concentration in ice cores. *Journal of Geophysical Research*, *111*(D15), D15107. https://doi.org/10.1029/2005jd006410

Fu, Q., White, R. H., Wang, M., Alexander, B., Solomon, S., Gettelman, A., et al. (2020). The Brewer-Dobson circulation during the Last Glacial Maximum. *Geophysical Research Letters*, *47*(5), e2019GL086271. https://doi.org/10.1029/2019GL086271

Gao, J., Korte, M., Panovska, S., Rong, Z., & Wei, Y. (2022). Effects of the Laschamps excursion on geomagnetic cutoff rigidities. *Geochemistry, Geophysics, Geosystems*, *23*(2), e2021GC010261. https://doi.org/10.1029/2021GC010261

Gieseler, J., Heber, B., & Herbst, K. (2017). An empirical modification of the force field approach to describe the modulation of galactic cosmic rays close to Earth in a broad range of rigidities. *Journal of Geophysical Research: Space Physics*, *122*(11), 10,964–10,979. https://doi.org/10.1002/2017JA024763

Gleeson, L. J., & Axford, W. I. (1968). Solar modulation of galactic cosmic rays. *The Astrophysical Journal*, *154*, 1011. https://doi.org/10.1086/149822

Heikkilä, U., Beer, J., & Feichter, J. (2009). Meridional transport and deposition of atmospheric ^{10}Be. *Atmospheric Chemistry and Physics*, *9*(2), 515–527. https://doi.org/10.5194/acp-9-515-2009

Heikkilä, U., Phipps, S. J., & Smith, A. M. (2013). ^{10}Be in late deglacial climate simulated by ECHAM5-HAM - Part 1: Climatological influences on ^{10}Be deposition. *Climate of the Past*, *9*(6), 2641–2649. https://doi.org/10.5194/cp-9-2641-2013

Herbst, K., Muscheler, R., & Heber, B. (2017). The new local interstellar spectra and their influence on the production rates of the cosmogenic radionuclides ^{10}Be and ^{14}C. *Journal of Geophysical Research: Space Physics*, *122*(1), 23–34. https://doi.org/10.1002/2016JA023207

Jackson, A., Jonkers, A. R. T., & Walker, M. R. (2000). Four centuries of geomagnetic secular variation from historical records. *Philosophical Transactions of the Royal Society of London, Series A: Mathematical, Physical and Engineering Sciences*, *358*(1768), 957–990. https://doi.org/10.1098/rsta.2000.0569

Kalnay, E., Kanamitsu, M., Kistler, R., Collins, W., Deaven, D., Gandin, L., et al. (1996). The NCEP/NCAR 40-year reanalysis project. *Bulletin of the American Meteorological Society*, *77*(3), 437–472. https://doi.org/10.1175/1520-0477(1996)077<0437:tnyrp>2.0.co;2

Köhler, P., Adolphi, F., Butzin, M., & Muscheler, R. (2022). Toward reconciling radiocarbon production rates with carbon cycle changes of the last 55,000 years. *Paleoceanography and Paleoclimatology*, *37*(2), e2021PA004314. https://doi.org/10.1029/2021pa004314

Koldobskiy, S. A., Bindi, V., Corti, C., Kovaltsov, G. A., & Usoskin, I. G. (2019). Validation of the neutron monitor yield function using data from AMS-02 experiment, 2011–2017. *Journal of Geophysical Research: Space Physics*, *124*(4), 2367–2379. https://doi.org/10.1029/2018JA026340

Korte, M., Brown, M. C., Panovska, S., & Wardinski, I. (2019). Robust characteristics of the Laschamp and Mono Lake geomagnetic excursions: Results from global field models [Dataset]. Frontiers of Earth Science, *7*(86). https://doi.org/10.3389/feart.2019.00086

Korte, M., & Constable, C. (2011). Improving geomagnetic field reconstructions for 0–3ka. *Physics of the Earth and Planetary Interiors*, *188*(3), 247–259. https://doi.org/10.1016/j.pepi.2011.06.017

Ku, T. L., Kusakabe, M., Measures, C. I., Southon, J. R., Cusimano, G., Vogel, J. S., et al. (1990). Beryllium isotope distribution in the Western North Atlantic: A comparison to the Pacific. *Deep-Sea Research, Part A: Oceanographic Research Papers*, *37*(5), 795–808. https://doi.org/10.1016/0198-0149(90)90007-I

Kusakabe, M., Ku, T. L., Southon, J. R., & Measures, C. I. (1990). Beryllium isotopes in the ocean. *Geochemical Journa*l, *24*(4), 263–272. https://doi.org/10.2343/geochemj.24.263

Laj, C., Kissel, C., & Beer, J. (2004). *High resolution global paleointensity stack since 75 kyr (GLOPIS-75) calibrated to absolute values* [Dataset]. In *Timescales of the paleomagnetic field* (pp. 255–265). American Geophysical Union. https://doi.org/10.1029/145GM19

Lal, D., & Peters, B. (1967). Cosmic ray produced radioactivity on the Earth. In K. Sitte (Ed.), *Kosmische strahlung II/cosmic rays II* (Vol. 9/46/2, pp. 551–612). Springer Berlin Heidelberg. https://doi.org/10.1007/978-3-642-46079-1_7

Lifton, N., Sato, T., & Dunai, T. J. (2014). Scaling in situ cosmogenic nuclide production rates using analytical approximations to atmospheric cosmic-ray fluxes. *Earth and Planetary Science Letters*, *386*, 149–160. https://doi.org/10.1016/j.epsl.2013.10.052

Liu, J., Nowaczyk, N. R., Panovska, S., Korte, M., & Arz, H. W. (2020). The Norwegian-Greenland Sea, the Laschamps, and the Monrjre excursions recorded in a Black Sea sedimentary sequence spanning from 68.9 to 14.5 ka [Dataset]. Journal of Geophysical Research: Solid Earth, *125*(8), e2019JB019225. https://doi.org/10.1029/2019JB019225

Mazaud, A., Laj, C., & Bender, M. (1994). A geomagnetic chronology for Antarctic ice accumulation. *Geophysical Research Letters*, *21*(5), 337–340. https://doi.org/10.1029/93GL02789

McCracken, K. G. (2004). Geomagnetic and atmospheric effects upon the cosmogenic ^{10}Be observed in polar ice. *Journal of Geophysical Research*, *109*(A4), A04101. https://doi.org/10.1029/2003JA010060

Mekhaldi, F., Muscheler, R., Adolphi, F., Aldahan, A., Beer, J., McConnell, J. R., et al. (2015). Multiradionuclide evidence for the solar origin of the cosmic-ray events of AD 774/5 and 993/4. *Nature Communications*, *6*(1), 8611. https://doi.org/10.1038/ncomms9611

Ménabréaz, L., Thouveny, N., Bourlès, D. L., Deschamps, P., Hamelin, B., & Demory, F. (2011). The Laschamp geomagnetic dipole low expressed as a cosmogenic ^{10}Be atmospheric overproduction at ~41ka. *Earth and Planetary Science Letters*, *312*(3–4), 305–317. https://doi.org/10.1016/j.epsl.2011.10.037

Miyake, F., Nagaya, K., Masuda, K., & Nakamura, T. (2012). A signature of cosmic-ray increase in AD 774-775 from tree rings in Japan. *Nature*, *486*(7402), 240–242. https://doi.org/10.1038/nature11123

Muscheler, R., Adolphi, F., Herbst, K., & Nilsson, A. (2016). The revised sunspot record in comparison to cosmogenic radionuclide-based solar activity reconstructions. *Solar Physics*, *291*(9–10), 1–19. https://doi.org/10.1007/s11207-016-0969-z

Muscheler, R., Beer, J., Kubik, P. W., & Synal, H. A. (2005). Geomagnetic field intensity during the last 60,000 years based on ^{10}Be and ^{36}Cl from the Summit ice cores and ^{14}C. *Quaternary Science Reviews*, *24*(16–17), 1849–1860. https://doi.org/10.1016/j.quascirev.2005.01.012

Muscheler, R., Beer, J., Wagner, G., Laj, C., Kissel, C., Raisbeck, G. M., et al. (2004). Changes in the carbon cycle during the last deglaciation as indicated by the comparison of ^{10}Be and ^{14}C records. *Earth and Planetary Science Letters*, *219*(3–4), 325–340. https://doi.org/10.1016/s0012-821x(03)00722-2

Nilsson, A., Holme, R., Korte, M., Suttie, N., & Hill, M. (2014). Reconstructing Holocene geomagnetic field variation: New methods, models and implications [Dataset]. Geophysical Journal International, *198*(1), 229–248. https://doi.org/10.1093/gji/ggu120

Nilsson, A., Suttie, N., Stoner, J. S., & Muscheler, R. (2022). Recurrent ancient geomagnetic field anomalies shed light on future evolution of the South Atlantic Anomaly [Dataset]. Proceedings of the National Academy of Sciences, *119*(24), e2200749119. https://doi.org/10.1073/pnas.2200749119

Paleari, C. I., Mekhaldi, F., Adolphi, F., Christl, M., Vockenhuber, C., Gautschi, P., et al. (2022). Cosmogenic radionuclides reveal an extreme solar particle storm near a solar minimum 9125 years BP. *Nature Communications*, *13*(1), 214. https://doi.org/10.1038/s41467-021-27891-4

Panovska, S., Korte, M., & Constable, C. G. (2019). One hundred thousand years of geomagnetic field evolution. *Reviews of Geophysics*, *57*(4), 1289–1337. https://doi.org/10.1029/2019RG000656

Panovska, S., Korte, M., Liu, J., & Nowaczyk, N. (2021). Global evolution and dynamics of the geomagnetic field in the 15–70 kyr period based on selected paleomagnetic sediment records [Dataset]. Journal of Geophysical Research: Solid Earth, *126*(12), e2021JB022681. https://doi.org/10.1029/2021JB022681

Pavón-Carrasco, F. J., Osete, M. L., Torta, J. M., & De Santis, A. (2014). A geomagnetic field model for the Holocene based on archaeomagnetic and lava flow data [Dataset]. Earth and Planetary Science Letters, *388*, 98–109. https://doi.org/10.1016/j.epsl.2013.11.046

Pedro, J. B., McConnell, J. R., van Ommen, T. D., Fink, D., Curran, M. A. J., Smith, A. M., et al. (2012). Solar and climate influences on ice core ^{10}Be records from Antarctica and Greenland during the neutron monitor era. *Earth and Planetary Science Letters*, *355*(356), 174–186. https://doi.org/10.1016/j.epsl.2012.08.038

Poluianov, S. V., Kovaltsov, G. A., Mishev, A. L., & Usoskin, I. G. (2016). Production of cosmogenic isotopes ^{7}Be, ^{10}Be, ^{14}C, ^{22}Na, and ^{36}Cl in the atmosphere: Altitudinal profiles of yield functions. [Dataset]. Journal of Geophysical Research: Atmospheres, *121*(13), 8125–8136. https://doi.org/10.1002/2016JD025034

Raisbeck, G. M., Yiou, F., Fruneau, M., Loiseaux, J. M., Lieuvin, M., & Ravel, J. C. (1981). Cosmogenic ^{10}Be/^{7}Be as a probe of atmospheric transport processes. *Geophysical Research Letters*, *8*(9), 1015–1018. https://doi.org/10.1029/GL008i009p01015

Roth, R., & Joos, F. (2013). A reconstruction of radiocarbon production and total solar irradiance from the Holocene ^{14}C and CO_2 records: Implications of data and model uncertainties. *Climate of the Past*, *9*(4), 1879–1909. https://doi.org/10.5194/cp-9-1879-2013

Siegenthaler, U., Heimann, M., & Oeschger, H. (1980). ^{14}C variations caused by changes in the global carbon cycle. *Radiocarbon*, *22*(2), 177–191. https://doi.org/10.1017/s0033822200009449

Simon, Q., Thouveny, N., Bourlès, D. L., Valet, J.-P., & Bassinot, F. (2020). Cosmogenic ^{10}Be production records reveal dynamics of geomagnetic dipole moment (GDM) over the Laschamp excursion (20–60 ka) [Dataset]. Earth and Planetary Science Letters, *550*, 116547. https://doi.org/10.1016/j.epsl.2020.116547

Simon, Q., Thouveny, N., Bourlès, D. L., Valet, J. P., Bassinot, F., Ménabréaz, L., et al. (2016). Authigenic ^{10}Be/^{9}Be ratio signatures of the cosmogenic nuclide production linked to geomagnetic dipole moment variation since the Brunhes/Matuyama boundary. *Journal of Geophysical Research: Solid Earth*, *121*(11), 7716–7741. https://doi.org/10.1002/2016JB013335

Snowball, I., & Muscheler, R. (2007). Palaeomagnetic intensity data: An achilles heel of solar activity reconstructions. *The Holocene*, *17*(6), 851–859. https://doi.org/10.1177/0959683607080531

Steig, E. J., Polissar, P. J., Stuiver, M., Grootes, P. M., & Finkel, R. C. (1996). Large amplitude solar modulation cycles of ^{10}Be in Antarctica: Implications for atmospheric mixing processes and interpretation of the ice core record. *Geophysical Research Letters*, *23*(5), 523–526. https://doi.org/10.1029/96GL00255

Steinhilber, F., Abreu, J. A., Beer, J., Brunner, I., Christl, M., Fischer, H., et al. (2012). 9,400 years of cosmic radiation and solar activity from ice cores and tree rings. *Proceedings of the National Academy of Sciences of the United States of America*, *109*(16), 5967–5971. https://doi.org/10.1073/pnas.1118965109

von Blanckenburg, F., O'Nions, R. K., Belshaw, N. S., Gibb, A., & Hein, J. R. (1996). Global distribution of beryllium isotopes in deep ocean water as derived from FeMn crusts. *Earth and Planetary Science Letters*, *141*(1), 213–226. https://doi.org/10.1016/0012-821X(96)00059-3

Vonmoos, M., Beer, J., & Muscheler, R. (2006). Large variations in Holocene solar activity: Constraints from ^{10}Be in the Greenland ice core project ice core. *Journal of Geophysical Research*, *111*(A10), A10105. https://doi.org/10.1029/2005ja011500

Webber, W. R., & Higbie, P. R. (2009). Galactic propagation of cosmic ray nuclei in a model with an increasing diffusion coefficient at low rigidities: A comparison of the new interstellar spectra with voyager data in the outer heliosphere. *Journal of Geophysical Research*, *114*(A2). https://doi.org/10.1029/2008JA013689

Wilks, D. S. (2006). In R. Dmowska, D. L. Hartmann, & T. Rossby (Eds.), *Statistical methods in atmospheric sciences* (2nd ed.). Academic Press.

Zheng, M., Adolphi, F., Sjolte, J., Aldahan, A., Possnert, G., Wu, M., et al. (2021). Solar activity of the past 100 years inferred from ^{10}Be in ice cores – Implications for long-term solar activity reconstructions. *Geophysical Research Letters*, *48*, e2020GL090896. https://doi.org/10.1029/2020GL090896

Zheng, M., Sturevik-Storm, A., Nilsson, A., Adolphi, F., Aldahan, A., Possnert, G., & Muscheler, R. (2021). Geomagnetic dipole moment variations for the last glacial period inferred from cosmogenic radionuclides in Greenland ice cores via disentangling the climate and production signals. *Quaternary Science Reviews*, *258*, 106881. https://doi.org/10.1016/j.quascirev.2021.106881

References From the Supporting Information

Baroni, M., Bard, E., Petit, J.-R., Magand, O., & Bourlès, D. (2011). Volcanic and solar activity, and atmospheric circulation influences on cosmogenic ^{10}Be fallout at Vostok and Concordia (Antarctica) over the last 60 years. *Geochimica et Cosmochimica Acta*, *75*(22), 7132–7145. https://doi.org/10.1016/j.gca.2011.09.002

Berggren, A. M., Beer, J., Possnert, G., Aldahan, A., Kubik, P., Christl, M., et al. (2009). A 600-year annual ^{10}Be record from the NGRIP ice core, Greenland. *Geophysical Research Letters*, *36*(11), L11801. https://doi.org/10.1029/2009gl038004

Usoskin, I. G., Gil, A., Kovaltsov, G. A., Mishev, A. L., & Mikhailov, V. V. (2017). Heliospheric modulation of cosmic rays during the neutron monitor era: Calibration using PAMELA data for 2006–2010. *Journal of Geophysical Research: Space Physics*, *122*(4), 3875–3887. https://doi.org/10.1002/2016JA023819

Zheng, M., Adolphi, F., Sjolte, J., Aldahan, A., Possnert, G., Wu, M., et al. (2020). Solar and climate signals revealed by seasonal ^{10}Be data from the NEEM ice core project for the neutron monitor period. *Earth and Planetary Science Letters*, *541*, 116273. https://doi.org/10.1016/j.epsl.2020.116273